ADVANCED FUNCTIONAL MATERIALS
www.afm-journal.de

A Zn-Doped CuO Nanocomposite Shows Enhanced Antibiofilm and Antibacterial Activities Against *Streptococcus Mutans* Compared to Nanosized CuO

Michal Eshed, Jonathan Lellouche, Aharon Gedanken, and Ehud Banin**

Zinc-doped copper oxide and copper oxide nanoparticles (NPs) are synthesized and deposited on artificial teeth by sonic irradiation, and the ability of these coatings to restrict biofilm formation by Streptococcus mutans is examined. The CuO and Zn:CuO NP-coated teeth show significant reductions in biofilm formation of 70% and 88%, respectively, compared to uncoated teeth. The mechanism of the Zn:CuO nanoparticles is investigated, revealing that the nanoparticles attach to and penetrate the bacteria and generate intracellular reactive oxygen species (ROS) that enhance lipid peroxidation and cause cell death. Conversely, the CuO or ZnO NPs do not show this behavior and could not generate intracellular ROS. These results highlight the superior efficacy of Zn:CuO nanocomposites over CuO and ZnO NPs and the role of ROS in their antimicrobial effect.

1. Introduction

Dental caries are a significant public health issue in children worldwide and represents the single most common childhood disease, with a rate of incidence that is five times higher than the next most prevalent disease, asthma.[1] In the US, 50% of children between the ages of 5 and 9 years have at least one cavity or filling, and this percentage increases to 78% among individuals who are 17 years old.[2] The human mouth provides an environment that is conducive to the colonization and growth of a diverse range of microorganisms of which bacteria are the most common.[3,4] Indeed, the human oral microbiome consists of a complex polymicrobial community that dwells in specific niches within the oral cavity and forms biofilms (plaque) on teeth, prostheses, and mucosal surfaces. Dental caries is caused by the demineralization of tooth enamel by the acids produced from dietary sugars by microorganisms growing in a biofilm or plaque.[5] Although the oral microbiota consist of hundreds of different organisms,[6] *Streptococcus mutans* (*S. mutans*) is the most potent cariogenic organism and is implicated in every type of dental caries.[7] Unfortunately, it is extremely difficult to eradicate dental biofilms, and simply brushing the teeth is not sufficient to remove these films. Therefore, the effective control of these pathogenic bacteria and dental plaque is critical to the prevention and treatment of oral disease, and drives the need for novel antimicrobial and antibiofilm agents. One approach is based on sonic irradiation, which is effective for the synthesis of nanophase materials and the deposition and insertion of nanoparticles (NPs) on/into mesoporous ceramic and polymer supports, fabrics, and glass.[8,9] In sonochemical synthesis, stable NPs are formed by the high energy released in the collapse of cavitation bubbles: this collapse creates conditions of very high temperature and pressure that lead to the rupture of chemical bonds. According to the proposed explanation for the sonochemical coating process, microjets form when acoustic bubbles collapse near a solid surface and propel newly formed NPs at a solid substrate at a high speed (>500 m/s) that is sufficient to embed the particles in the substrate.[10]

We recently reported the sonochemical synthesis of a Zn-doped CuO composite ($Cu_{0.88}Zn_{0.12}O$, designated Zn:CuO).[11] The Zn^{2+} ions are doped in the unit cell of the monoclinic CuO lattice, replacing Cu^{2+} ions and thus forming doped particles. These NPs show excellent antibacterial properties that are 10 000–100 000 times stronger than CuO or ZnO against *Escherichia coli* (Gram negative) and *Staphylococcus aureus* (Gram positive) bacteria. Similar activities were even observed for multidrug-resistant (MDR) bacteria (i.e., methicillin-resistant *S. aureus* and MDR *E. coli*), further emphasizing the efficacy of this composite material. However, the antibacterial and antibiofilm activities of Zn-doped CuO against *S. mutans* have not yet been reported; furthermore, to the best of our knowledge, there are almost no studies of the antibacterial and antibiofilm activities of doped or mixed metal oxides. We previously reported the effects of CuO and ZnO on the formation of oral biofilms, and our results showed that CuO and ZnO do not kill *S. mutans* but rather prevent the formation of *S. mutans* biofilms.[12] Accordingly, the objective of the present study was

M. Eshed, Dr. J. Lellouche, Prof. A. Gedanken
Department of Chemistry
The Bar-Ilan Institute of Nanotechnology
and Advanced Materials
Bar-Ilan University
Ramat-Gan, 52900, Israel
E-mail: aharon.gedanken@biu.ac.il
Dr. J. Lellouche, Dr. E. Banin
The Biofilm Research Laboratory
The Bar-Ilan Institute of Nanotechnology and Advanced Materials
The Mina and Everard Goodman Faculty of Life Sciences
Bar-Ilan University
Ramat-Gan, 52900, Israel
E-mail: ehud.banin@biu.ac.il

DOI: 10.1002/adfm.201302425

to contrast the antibiofilm and antibacterial activities of Zn:CuO and CuO NPs. An unexpected result was that the Zn-doped CuO composite NPs exhibited some antibacterial activity against *S. mutans*, which enhanced the antibiofilm activity of these NPs. We also examined the interaction of both types of NPs with *S. mutans* cells. The generation of intracellular reactive oxygen species (ROS), a typical property of metal oxide nanoparticles, and lipid peroxidation were measured using different assays for the Zn:CuO and CuO NPs.

2. Results and Discussion

2.1. Characterization and Antibiofilm Properties of Zn:CuO and CuO NP-Coated Surfaces

A high-resolution scanning electron microscopy (HR-SEM) analysis was performed to examine the coatings formed on tooth surfaces using sonochemical methods. **Figure 1**B and C illustrate the Zn:CuO and CuO NP coatings, respectively, on tooth surfaces. The sonication reaction created a uniform coating over the bare tooth (Figure 1A), and the average particle diameter were approximately 30 and 70 nm for Zn:CuO and CuO NPs, respectively (Figure 1D and E).

The presence of Zn:CuO and CuO NPs on tooth surfaces and the penetration depth profiles were also examined by Rutherford backscattering spectrometry (RBS). Figure 1G and H reveal the presence of elemental Cu, as indicated with an arrow, on teeth. In the case of a tooth coated with Zn:CuO NPs, the Zn^{2+} ions are doped in the unit cell of the monoclinic CuO lattice and their negligible concentration in the lattice was not detected. The peak observed in Figure 1G is attributed solely to elemental Cu. A comparison of Figure 1F,G,H confirms the successful formation of coatings on these tooth surfaces.

We next examined whether NPs formed surface deposits or penetrated the tooth surfaces. The RBS technique, which is based on the deceleration of ions in matter to provide depth resolution, was utilized to compare the penetration depths of the Zn:CuO and CuO NPs in tooth surfaces. The results presented in **Figure 2** indicate the following: (i) Zn:CuO NP and CuO NP coating layers formed, but there were variations in the NP coating thickness; (ii) deeper penetration into the tooth was detected for the Zn:CuO NPs coating (over 1500×10^{15} atoms/cm^2); and (iii) more Cu was obtained with Zn:CuO versus CuO NP coatings. It should be noted that the minor amounts of Zn^{2+} were not detected by RBS.

The focused ion beam scanning electron microscopy (FIB-SEM) technique was used to examine the coating layers of both types of NPs on the tooth surfaces. FIB milling was applied to

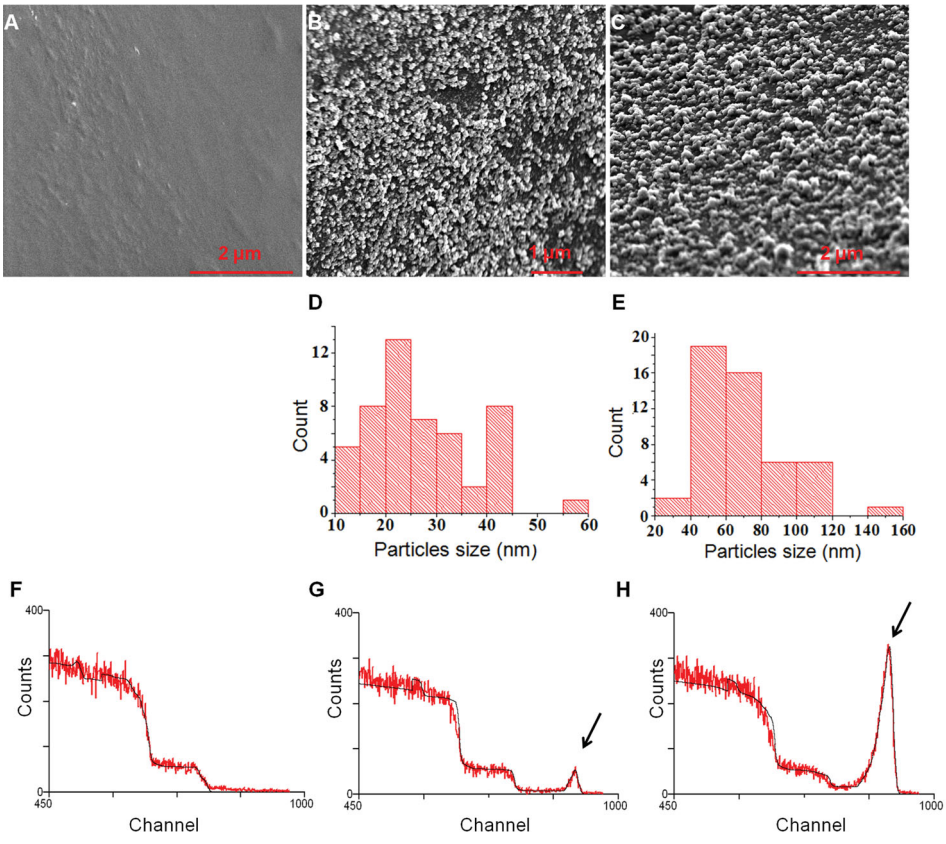

Figure 1. Imaging of sonochemical Zn:CuO and CuO NP tooth coatings. Teeth were coated using the sonochemical procedure described in the experimental section. HR-SEM images with the same magnification: A) the surface of an uncoated tooth; B) a tooth surface coated with Zn:CuO NPs; C) a tooth surface coated with CuO NPs; the size distribution of D) Zn:CuO NPs and E) CuO NPs present on the tooth surfaces. The RBS spectra for F) an uncoated tooth, G) a tooth coated with Zn:CuO NPs, and H) a tooth coated with CuO NPs. (Red) measured and (black) simulated results.

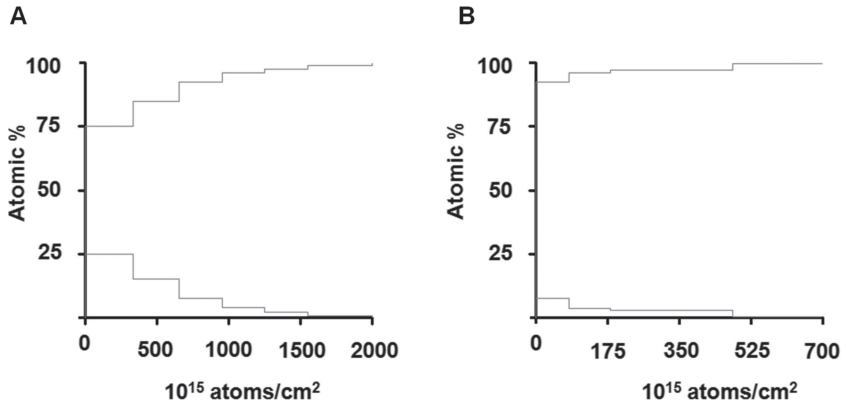

Figure 2. RBS compositional depth profiles. A) A tooth coated with Zn:CuO NPs and B) a tooth coated with CuO NPs. (Upper graph) substrate, tooth; (lower graph) NP coating.

inspect the deposit structure/thickness in the cross-section of a plateau-honed groove, as shown in **Figure 3**. The FIB data indicate that NP layers cover the tooth surface: the control tooth shows the absence of a particle coating (Figure 3A), whereas the teeth coated with Zn:CuO or CuO NPs show particle layers (Figure 3B and C). Figure 3B and C show the continuous coatings of Zn:CuO and CuO NPs, which are 53.9 and 44.6 nm thick, respectively, along the grooves on the tooth surfaces.

The atomic ratio of Cu:Zn in the free nanocomposites was previously found to be Cu^{2+}:Zn^{2+} = 8:1.[11] We thus investigated whether this ratio was maintained on the teeth coated with the Zn:CuO compound by treating the coated teeth with HNO_3 and measuring the concentrations of Zn^{2+} and Cu^{2+} ions using inductively coupled plasma (ICP). In agreement with previous data, the ratio of Cu:Zn deposited on the tooth surface was found to be 8:1.

Next, we examined the ability of the Zn:CuO and CuO NP-coated surfaces to inhibit *S. mutans* bacterial colonization. Using a static biofilm assay, teeth were challenged for 24 h in the presence of *S. mutans*, and the biofilm biomass was quantified. As observed in **Figure 4**A, there was a massive biofilm on the uncoated tooth, whereas biofilm formation was reduced by 88% and 70% on the teeth coated with the Zn:CuO and CuO NPs, respectively (Figure 4A). We performed a one-way analysis of variance (ANOVA) between the three groups, and the results indicated a significant difference ($F_{(2,6)}$ = 336.32, $p < 0.001$). We also used a post-hoc Scheffe test, which indicated that the biofilm was significantly smaller for the Zn:CuO coating (mean [M] = 0.1, standard deviation [SD] = 0.24) than the control (M = 0.87, SD = 0.04) and the CuO coating (M = 0.29, SD = 0.05). Additionally, the effectiveness of the Zn:CuO and CuO NP-coated surfaces in inhibiting *S. mutans* was supported by the HR-SEM images (Figure 4B), as no *S. mutans* biofilm formation was observed on the teeth coated with Zn:CuO and CuO NPs.

In this study, the CuO NP-coated teeth did not affect planktonic growth (Figure 4C), which was consistent with our previous studies,[12] though the Zn:CuO NP coating did slightly reduce the growth of planktonic *S. mutans*. A one-way ANOVA was performed among the three groups, and the results indicated a significant difference ($F_{(2,6)}$ = 47.66, $p < 0.001$). A post-hoc Scheffe test on data for planktonic growth indicated that there was no significant difference between the control (M = 1.56, SD = 0.06) and CuO (M = 1.55, SD = 0.04), whereas the Zn:CuO (M = 1.26, SD = 0.32) was significantly lower than the control. This finding implies that Zn:CuO NPs have an antimicrobial activity against *S. mutans* planktonic cultures, which will be discussed in detail below.

2.2. Antibacterial Properties of Zn:CuO and CuO Nanoparticles

To characterize the antimicrobial activity of Zn:CuO and CuO NPs, the growth of *S. mutans* with free NPs was examined (**Figure 5**). As was observed with the coated teeth, free CuO NPs did not impact the growth of *S. mutans* (Figure 5A). The Zn:CuO NPs did not completely inhibit bacterial growth but delayed growth and reduced the viability of *S. mutans* from 1.7×10^8 CFU/mL to 6.3×10^6 CFU/mL (Figure 5B). A one-way ANOVA indicated a significant difference ($F_{(2,6)}$ = 171.56, $p < 0.001$). As shown by the growth curves, the CuO-treated samples did not show a significant decrease in bacterial viability.

A major obstacle in NP utilization that could affect their antimicrobial activity is the tendency of solid NPs to dissolve (very small K_{sp}) and release very small amounts of ions into the medium (K_{sp} of CuO is 10^{-20}). However, it is possible that Zn:CuO particles do not behave in the same way. For example, if the concentration of Cu^{2+} ions released from Zn:CuO NPs is greater than the concentration of Cu^{2+} released from CuO NPs, it can be argued that

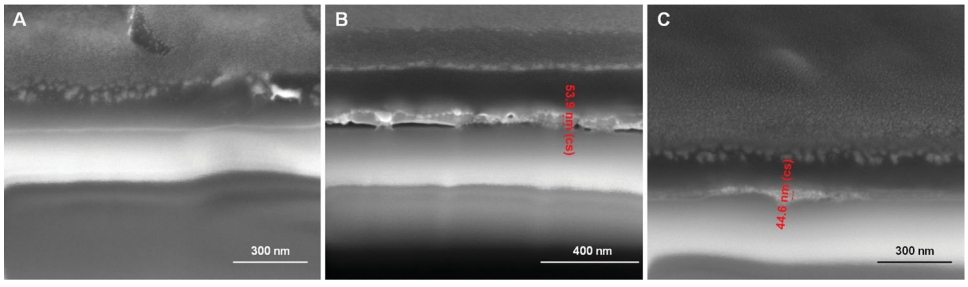

Figure 3. FIB-SEM images of the samples: A) An uncoated tooth, B) a tooth coated with Zn:CuO, and C) a tooth coated with CuO. The white coating on the top of each of these three samples is the platinum layer, which was deposited to protect the surface from accidental ion beam damage.

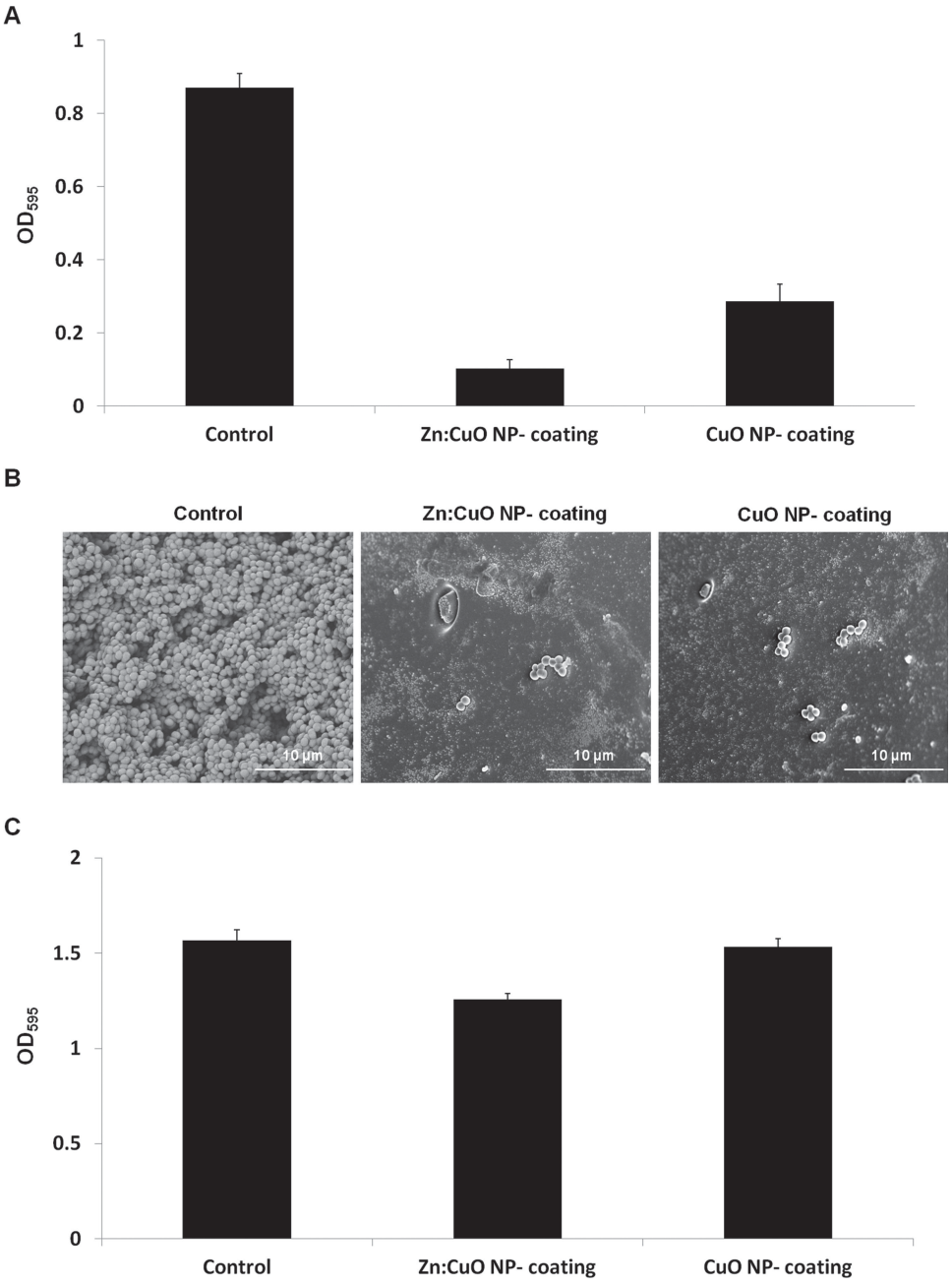

Figure 4. Zn:CuO and CuO NP-coated teeth restrict *S. mutans* biofilm formation. A) Quantification of the biofilm biomass developed after incubation with *S. mutans* for 24 h. The biofilm was stained with crystal violet as described in the experimental section. B) HR-SEM imaging of *S. mutans* biofilms on coated and uncoated teeth. Biofilms were grown for 24 h at 37 °C. C) Planktonic growth. The error bars represent the standard deviation of three independent experiments performed in triplicate.

the Cu^{2+} ions are responsible for the antibacterial activity of the Zn:CuO NPs. Cu^{2+} ions are a potent inhibitor of several enzymes and metabolic pathways in bacterial cells,[13] and Cu^{2+} ions can combine with the membrane by electrostatic attraction and penetrate the cell through membrane channels. Once inside the cell, Cu^{2+} can strongly combine with intracellular sulfur-containing amino acids, leading to the denaturation of proteins and possibly resulting in cell death. Several studies have demonstrated the efficacy of Cu^{2+} in reducing plaque formation in humans and in inhibiting the ability to generate acid after exposure to sucrose,[14–16] and this antimicrobial activity has been attributed to the oxidation of critical thiol groups in bacterial enzymes by Cu^{2+}.[17] According to the literature,[14,18] when 1 mmol/L Cu^{2+} was included in drinking water, rats infected with *S. mutans* had significantly fewer experimental caries, and substantially lower populations of *S. mutans* colonized their tooth surfaces. In the case of Zn^{2+} ions, it has been reported that a higher Zn^{2+} content has a pronounced effect against pathogens.[19]

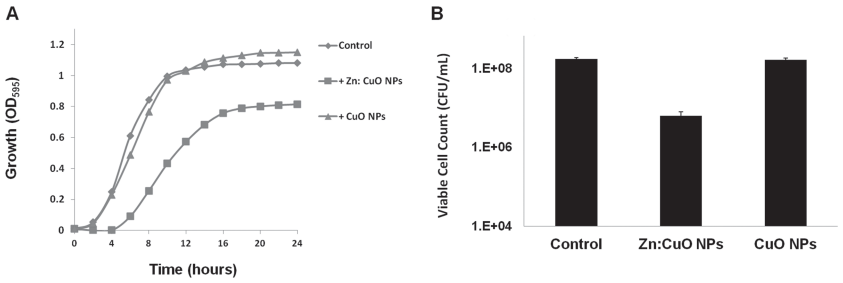

Figure 5. Effect of Zn:CuO and CuO NPs on *S. mutans* growth. A) Growth curves of *S. mutans* exposed to Zn:CuO (1 mg/mL) and CuO NPs (1 mg/mL) for 24 h at 37 °C. Untreated bacteria served as a negative control. B) Viability of *S. mutans* after exposure to Zn:CuO and CuO NPs (1 mg/mL) or CuO NPs (1 mg/mL) after 24 h. The error bars represent the standard deviation of three independent experiments performed in triplicate.

The effects of such metal ions as Zn^{2+} and Cu^{2+} on glucosyltransferases have also been reported.[20] Glucosyltransferase activity mediates the sucrose-dependent adherence of *S. mutans* to the tooth surface, which is essential for the cariogenicity of these microorganisms, and contributes significantly to the exopolysaccharide component of the dental-plaque matrix. As the cations Zn^{2+} and Cu^{2+} significantly inhibit glucosyltransferases, Cu^{2+} and Zn^{2+} affect the colonization of tooth surfaces by cariogenic bacteria by inhibiting bacterial metabolism and subsequent bacterial growth. We first measured the concentrations of Zn^{2+} and Cu^{2+} ions released from Zn:CuO and CuO NPs (1 mg/mL) in brain-heart (BH) medium after 24 h (**Table 1**). After identifying the exact concentrations released from the particles, we investigated whether the Cu^{2+} and Zn^{2+} ions released from the NPs are responsible for the observed antibacterial behavior (Figure 5). The growth of *S. mutans* in media inoculated with either Cu^{2+} or Zn^{2+} ions was examined at the concentrations presented in Table 1 over a period of 24 h (**Figure 6**). Although the concentrations of Zn^{2+} and Cu^{2+} used in this experiment were not toxic to the *S. mutans* culture, we sought to determine that the antibacterial activity was not mediated by the release of Zn^{2+} ions. Therefore, we added Zn^{2+} (the concentration from Table 1) to the CuO NPs (1 mg/mL); again, no antibacterial activity was observed, as in the cases of Cu^{2+} and Zn^{2+} ions (Figure 6). Based on these results, it is clear that the primary factor in the antibacterial action of Zn:CuO NPs is related to the structure of the nanocomposite rather than to soluble zinc or copper ions.

2.3. Interaction of Zn:CuO and CuO Nanoparticles with Bacteria Cells

Disorganization of the membrane by undesired or foreign substances can cause the loss of membrane integrity, which leads to membrane permeability malfunction,[21] with the loss of membrane permeability ultimately leading to cell death. In a further effort to understand the antibacterial activity of Zn:CuO particles compared to CuO particles, we utilized transmission electron microscopy (TEM) measurements to examine the effect of the nanoparticles on bacteria. *S. mutans* cells, both untreated and treated with CuO NPs (**Figure 7**), showed a normal cell morphology, with the distinct cell walls and membrane structures typical of uninjured Gram-positive bacteria. However, the Zn:CuO NP-treated samples of *S. mutans* cells (Figure 7) exhibited the nanoparticles localized either on the cell surface or within the cell membrane. Moreover, in the case of the Zn:CuO NPs, the cell membrane appeared to be damaged and disorganized, whereas the cell membrane in the case of the CuO NPs remained intact, without visible injury. We should emphasize that some of the particles remained attached to the cell membrane, even after the bacteria had been washed prior to fixation for microscopic examination. The ability of nanoparticles to penetrate into cells has been demonstrated with other nanoparticles, such as ZnO,[22] MgO,[23] and MgF_2[21] NPs.

To further investigate the penetration of the Zn:CuO composites into bacteria, we measured the intracellular levels of Cu and Zn following exposure. The results presented in **Table 2** suggest that the exposure to Zn:CuO NPs caused a dramatic increase in Cu within the cells compared to the exposure to CuO NPs. The ratio between Cu and Zn was very close to 8:1, further supporting the internalization of NPs with this ratio.

The fact that the Zn:CuO nanoparticles were observed at the surfaces of the cell membranes may impact the zeta potential, which affects antimicrobial activity.[24] Our zeta potential measurements (**Figure 8**) revealed that the average charges of the Zn:CuO NPs and CuO NPs were –12 mV and –13.9 mV, respectively. Although a strongly positive zeta potential promotes the interactions of an NP with the cell membrane, the Zn:CuO particles that had a negative zeta potential, promoted

Table 1. Cu^{2+} and Zn^{2+} ion concentrations released from CuO and Zn:CuO NPs after immersion in BH medium for 24 h (by inductively coupled plasma (ICP)).

	$[Cu^{2+}]$ mg/L	$[Zn^{2+}]$ mg/L
Zn:CuO NPs	99.46	0.58
CuO NPs	99.76	–

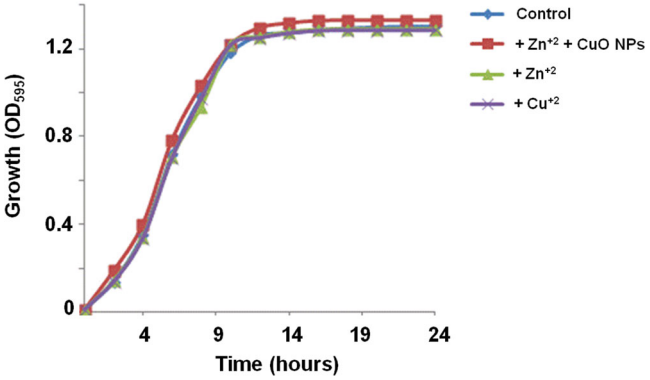

Figure 6. Effect of Zn^{2+}, Cu^{2+}, and Zn^{2+}+CuO NPs on *S. mutans* growth. Growth curves of *S. mutans* exposed to Zn^{2+}, Cu^{2+}, and a mixture of Zn^{2+} and CuO NPs at the concentrations indicated in the text for 24 h at 37 °C. Untreated bacteria served as the negative control.

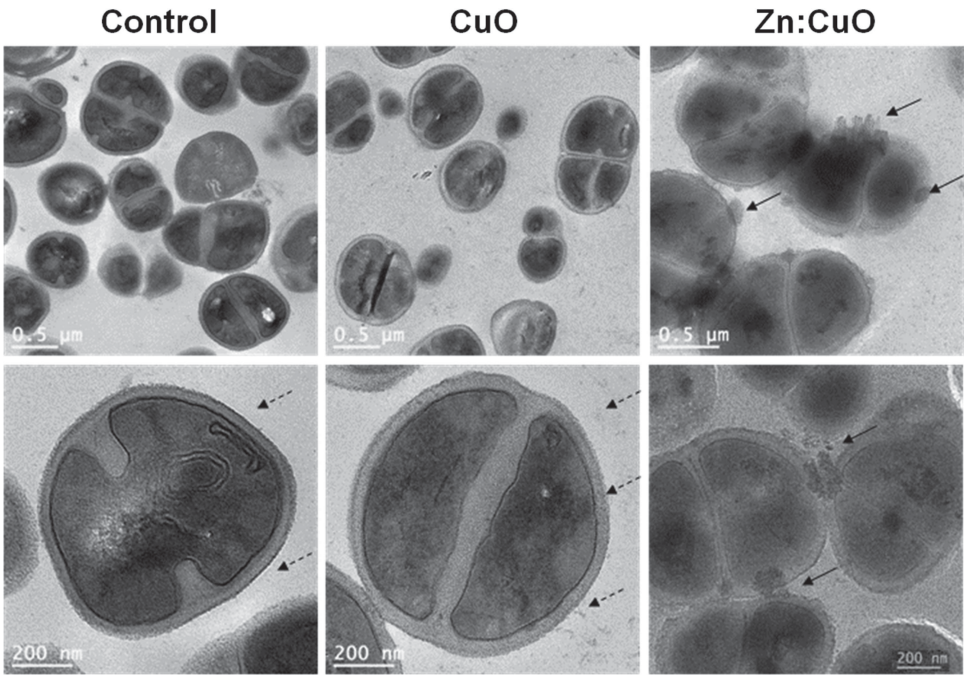

Figure 7. Transmission electron microscopy. Treated cells with Zn:CuO (1 mg/mL) and CuO NPs (1 mg/mL) and untreated *S. mutans* cells. The dashed arrows indicate normal cell membranes; the unbroken arrows indicate Zn:CuO nanoparticles.

interactions with cell membranes (Figure 7) and penetrated into the bacteria cells (Table 2). The negative zeta potential of the nanoparticles and the minimal electrostatic interactions of the particles with the negatively charged bacterial surface may explain why a relatively high concentration of nanoparticles was necessary to produce an antibacterial effect.

2.4. Intracellular ROS Concentration

Another possible mechanism for the antimicrobial activity of NPs is the production of ROS. To identify the existence of ROS inside bacterial cells upon exposure to Zn:CuO and CuO NPs and to compare these results with a suspension of *S. mutans* without NPs, H_2DCFDA [5-(and 6-)chloromethyl-2,7-dichlorodihydrofluorescein diacetate, acetyl ester] was used as described in the Experimental Section. In the presence of ROS, the dye is oxidized to the fluorescent dichlorofluorescein (DCF); as the ROS concentration in the cell increases, the fluorescent intensity of DCF also increases. **Figure 9** illustrates the ROS

Table 2. Intracellular concentrations of Cu^{2+} and Zn^{2+} following exposure to either Zn:CuO or CuO NPs. The concentrations were detected after lysis of the *S. mutans* cells. The CuO and Zn:CuO NP powders were immersed in BH medium for 24 h.

	[Cu^{2+}] µg/L	[Zn^{2+}] µg/L
S. mutans	5	–
S. mutans + Zn:CuO NPs	327.6	42.86
S. mutans + CuO NPs	19.9	–

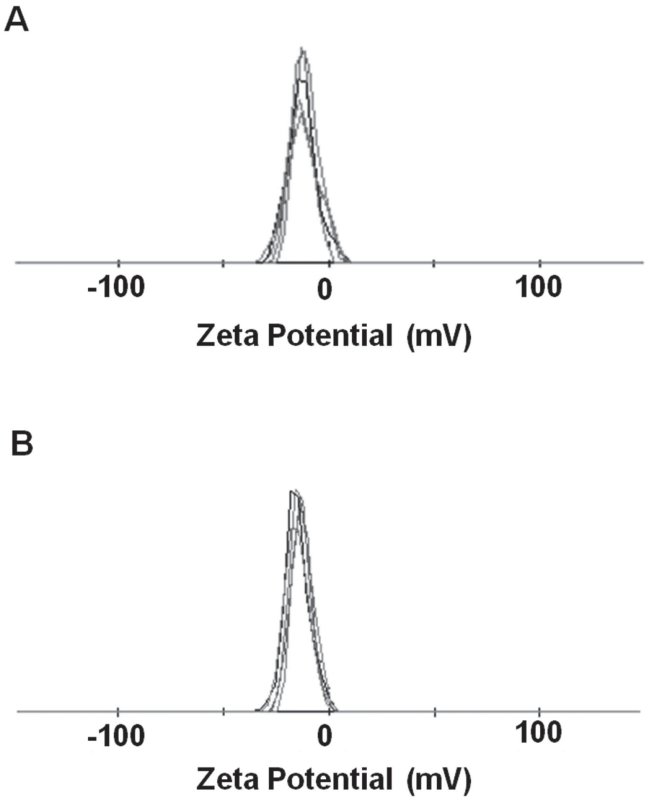

Figure 8. Zeta potential of A) Zn:CuO NPs in BH medium and B) CuO NPs in BH medium. The different lines indicate the measurements of several independent samples.

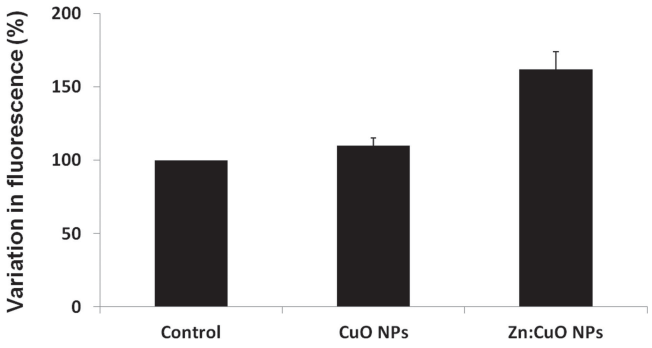

Figure 9. Intracellular ROS detection assay. No intracellular ROS generation was detected in the control sample, very little intracellular ROS was observed when CuO NPs were added, and increased fluorescence intensity was observed when Zn:CuO NPs were added. The error bars represent the standard deviation of three independent experiments performed in triplicate. A one-way ANOVA was performed among the three groups, and the results indicated a significant difference ($F_{(2,6)} = 45.05$, $p < 0.001$). Post-hoc Scheffe test results indicated a significantly higher value for Zn:CuO (M = 161.83, SD = 12) than the control (M = 100, SD = 0) and CuO (M = 110, SD = 8.7). There was no significant difference between the control and CuO sample.

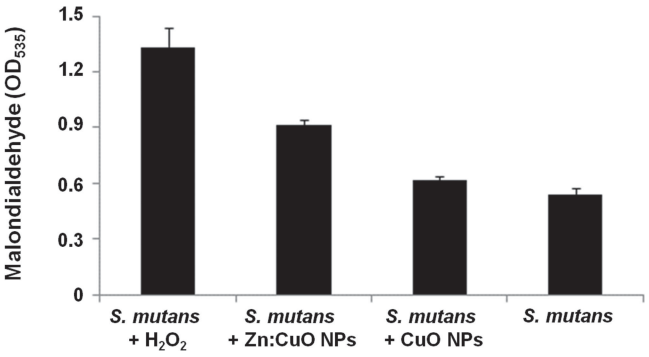

Figure 10. Effects of Zn:CuO NPs and CuO NPs on lipid peroxidation. The oxidative degradation of membrane lipids in *S. mutans* cultures exposed to 1 mg/mL of Zn:CuO NPs and CuO NPs was monitored by MDA concentrations, as described in the experimental section. Untreated samples of *S. mutans* and H_2O_2 (1 mM) served as controls. A one-way ANOVA was performed among the four groups, and the results indicated a significant difference ($F_{(3,8)} = 111.18$, $p < 0.001$). A post-hoc Scheffe test indicated a significantly higher value for H_2O_2 (M = 1.33, SD = 0.11) than *S. mutans* alone (M = 0.53, SD = 0.04) and *S. mutans* + CuO NPs (M = 0.62, SD = 0.02) and *S. mutans* + Zn:CuO NPs (M = 0.91, SD = 0.03). The value for *S. mutans* + Zn:CuO NPs was significantly higher than the untreated *S. mutans* control and *S. mutans* + CuO NPs. There was no significant difference between *S. mutans* and *S. mutans* + CuO NPs.

concentration of samples containing the Zn:CuO and CuO NPs, revealing a slight increase in fluorescence intensity in the cells treated with the CuO NPs compared to the untreated control. This result, for CuO, indicates a smaller presence of ROS inside the cells, and this low concentration of ROS is apparently unable to cause sufficient damage to kill *S. mutans* cells. A more dramatic effect was observed for the cells treated with the Zn:CuO NPs relative to the untreated control, whereby the emitted green fluorescence increased by approximately 62%. Thus, we concluded that the intracellular ROS, is associated with the antibacterial effect.

2.5. Effect of Zn:CuO and CuO Nanoparticles on Membrane Lipid Peroxidation

Lipid peroxidation is a signature of ROS damage, which often occurs in response to oxidative stress and leads to lipid hydroperoxide formation. Lipids contain polyunsaturated fatty acids that are susceptible to free radical-initiated oxidation and can participate in chain reactions that increase damage to biomolecules.[25] Lipid peroxidation can be detected by assaying malondialdehyde (MDA), an oxidation product of polyunsaturated fatty acids and a metabolic marker for lipid peroxidation and metabolic cell damage.[26] MDA forms an adduct with thiobarbituric acid (TBA), resulting in a product with increased absorbance at 535 nm.[26] To determine the effect of the Zn:CuO and CuO NPs on membrane lipid peroxidation, we monitored MDA production by *S. mutans* with and without the exposure to both types of NPs (1 mg/mL). As shown in **Figure 10**, the addition of Zn:CuO NPs increased the MDA concentration in the cells to a level that was higher than the amount produced by the same concentration of CuO.

The combination of the ability of many NPs to generate ROS and their direct contact with cells is considered to be the major mechanism by which these NPs produce their toxic effects.[27–29] We propose that these two essential requirements also apply to the systems considered in this study, i.e., the strong adherence of the particles to the bacterial cell membrane, only in the case of the Zn:CuO NPs, and ROS generation that damages the cells.

3. Conclusions

The present study presents the synthesis and coating of Zn:CuO and CuO NPs on teeth using a simple sonochemical process. Our results revealed that this ultrasonic technique provides an active antibiofilm coating on tooth surfaces. The teeth coated with Zn:CuO and CuO NPs show significant reductions in biofilm formation, by 88% and 70%, respectively, compared to uncoated teeth, which supported massive biofilm formation. Only the Zn:CuO NPs demonstrated antibacterial activity against *S. mutans*, whereas the CuO NPs did not show this effect. Electron spectroscopy showed that the Zn:CuO NPs tended to adhere to cell surfaces and disrupt the cell membrane integrity, and we attributed the antibacterial activity to intracellular ROS generation induced by Zn:CuO NPs. The results of the present study further highlight the potential of these novel Zn:CuO NPs as inhibitors of biofilm formation within the context of the oral niche.

4. Experimental Section

Zn:CuO and CuO NP Synthesis and Coating Procedure: To obtain the $Cu_{0.88}Zn_{0.12}O$, Zn:CuO NPs, the molar ratio of reagent-grade zinc and copper acetates were mixed in the aqueous solution with a Cu:Zn ratio of 3:1. Copper acetate monohydrate was dissolved in 10 mL of

doubly distilled water (ddH_2O), and zinc acetate dihydrate was added; the concentrations of Cu^{2+} and Zn^{2+} were 0.0075 M and 0.0025 M, respectively. Ethanol was added to this solution to a final volume of 100 mL. After 5 min of sonication, 0.8 mL of an aqueous solution of ammonium hydroxide (28–30%) was injected into the reaction cell to adjust the pH to approximately 8. The solution was chilled in a water bath, keeping the temperature at 30 °C. The sonochemical deposition process continued for 30 min using a high-intensity ultrasonic horn (Ti horn, 20 kHz, 750 W at 60% efficiency). To prepare the CuO NPs, copper acetate was used at the same concentration as for the synthesis of the Zn:CuO NPs (0.0075 M). Copper acetate was dissolved in 10 mL of doubly distilled water, and ethanol was added to a final volume of 100 mL. Ammonium hydroxide (28–30%) was added until the pH of the solution was approximately 8. The reaction mixture was irradiated for 30 min with a high-intensity ultrasonic horn (as above), and the sonication vessel was cooled at a constant temperature of 30 °C. Both solutions were centrifuged, and the NP precipitates were washed twice with ddH_2O and then with ethanol; the solutions were then dried under vacuum.

NP coatings were obtained by placing an artificial acryl tooth (obtained from the School of Dental Medicine at the Tel Aviv University) directly into the sonochemical reaction medium according to the methodology described above. The tooth was held by a wire to keep it at a constant distance of 2 cm from the sonicator tip during the entire reaction process. The atomic ratio of Cu:Zn on the tooth surface was determined indirectly by ICP (ULTIMA 2, Horiba Scientific). The teeth that were coated with Zn:CuO NPs were washed three times with ddH_2O and then immersed in strong acid (HNO_3) to dissolve the zinc and copper oxides; the ion concentrations in the solution were determined by ICP. To analyze the coating morphologies, the samples were coated with chromium and imaged by HR-SEM (JEOL-6700F, accelerating voltage 15 kV). The size distribution of the NPs was determined from the measurement of images captured with HR-SEM (n = 100).

An FIB technique was employed to analyze the coating cross-sections using a dual beam system (Helios 600, FEI) with electron and ion beams up to 30 kV. The combination of two beams at different angles (52 degrees) enables simultaneous measurements.

To examine the existence of NPs on tooth surfaces and the penetration of the NPs into the teeth, an RBS was performed using a 1.7 MV Pelletron accelerator from NEC (commissioned during summer 2011 at the BINA, Bar Ilan University). This instrument is capable of generating proton beams up to 3.4 MeV and alpha particle beams up to 5.1 MeV.[30] For each sample, an RBS spectrum was acquired with a fixed detector (ULTRA Silicon-Charged Particle Detector, ORTEC). For each sample, a 5-μC spectrum was collected with a 2.022 MeV ± 1 KeV $4He^+$ beam; the nominal diameter of the beam is 2 mm. An electron suppressor was used between the beam entrance and the sample holder, which was biased at –100 V vs. ground. The scattering angle of the fixed detector was 169°, and solid angle was 2.7 msr. A normal incident beam was used in all measurements. Every sample was mounted in the holder using double-sided, self-adhesive carbon tape. The NDFv9.4e software was used to fit the data.[31] We also used SRIM 2003 stopping powers.[32] We employed the double-scattering calculation in NDF,[33] which gives a surprisingly good fit of the low-energy signal; the pulse pileup calculation in NDF uses the algorithm of Wielopolsky & Gardner.[34] Enhanced backscattering spectroscopy (EBS) was used to make small corrections for O and C in the cross-sections. The EBS (non-Rutherford) scattering cross-sections were obtained from IBANDL.[35,36] SigmaCalc was used for evaluating cross-sections (e.g., C, N, O, Si)[37,38] NDFv9.3e was implemented to interpolate data of tables derived from SigmaCalc. Depth profiles can be extracted automatically from RBS, EBS, ERD, and NRA spectra using the Surrey IBA DataFurnace software.[39,40] We validated the accuracy of this code against a certified standard sample[41] and by an international comparison study.[42]

Bacterial Cultures and Growth Conditions: In every experiment, *S. mutans* 700610 (clinical isolate) was grown aerobically at 37 °C in Brain–heart medium supplemented with 0.5% sucrose (noted BH), which induces robust biofilm formation.[43]

Antibacterial Test: Overnight Cultures of tested bacteria were diluted (1:100) in fresh media, grown for 8 h at 37 °C (shaking, 250 rpm). The water-insoluble compounds were assayed in a modified macro-dilution assay. The Zn:CuO and CuO NPs, Zn^{2+} and Cu^{2+} ions, and mixtures of Zn^{2+} ions and CuO NPs at various concentrations (see above) were added to sterile polypropylene tubes (Greiner Bio-One), and the appropriate volume of a 0.01 OD_{595} solution (approximately 10^7 CFU/mL) of *S. mutans* culture was added. For each tested cell suspension, 100 μL was then added to a well in a 96-well plate that was incubated for 24 h at 37 °C. Following incubation, the bacterial growth was determined spectrophotometrically by measuring the absorbance at 595 nm (OD_{595}, Synergy 2, BioTek Instruments).

Biofilm Assays on Artificial Teeth: Artificial teeth were assayed using a static biofilm assay. Artificial teeth were placed in a 24-well plate (Greiner Bio-One); each well contained a 3 mL bacterial suspension of *S. mutans* at a final concentration of OD_{595} = 0.15 (approximately 1.5×10^8 CFU/mL) in BH medium. After incubating for 24 h at 37 °C, the teeth were washed twice with ddH_2O to remove the non-attached cells, and the biofilm biomass was stained with 1% crystal violet (CV, Sigma) for 15 min at room temperature. The stained biofilm that formed on the teeth was washed five times with ddH_2O, and the remaining CV was eluted with absolute ethanol for 15 min. The biofilm biomass was then determined by measuring the absorbance at OD_{595}.

To examine the biofilm morphology, teeth samples were exposed after incubation to Karnovsky's fixative (glutaraldehyde + paraformaldehyde) for 1 h. The samples were washed three times with phosphate-buffered saline (PBS) without Ca^{2+} and Mg^{2+}. The samples were immersed for 1 h in a mixture of titanic acid and a glutamate solution in a 4:5 concentration ratio. After three cycles of washing with PBS, the samples were exposed to an osmium tetraoxide solution for 1 h. Lastly, the residual water was removed with water-ethanol and ethanol-freon solutions (from 50% to 100% of each solvent). The samples were then dried in air, carbon-coated, and imaged by HR-SEM (JEOL-6700F, accelerating voltage of 15 kV).

Transmission Electron Microscopy (TEM) of Bacterial Samples: Samples of *S. mutans* cultures were centrifuged and washed immediately after 24 h of treatment with and without Zn:CuO and CuO nanoparticles (1 mg/mL). The samples were fixed in 25% glutaraldehyde/paraformaldehyde in cacodylate buffer at room temperature for 1 h. The samples were washed with cacodylate buffer and then fixed in 1% osmium tetraoxide.

Sample embedding was performed using a standard protocol described elsewhere,[44] and 60 nm thick slices were cut using a diamond knife (LBR ultratome III). The slices were deposited on bare 200-mesh copper grids and stained with 2 wt% uranyl acetate for 5 min. The grids were dried in a desiccator and examined using a JEOL 1200Ex transmission electron microscope.

Penetration of Nanoparticles into the Bacteria Cells: S. mutans at a final concentration of OD_{595} = 0.15 (approximately 1.5×10^8 CFU/mL) in BH medium was suspended with 1 mg/mL CuO or Zn:CuO NPs. After 24 h of incubation at 37 °C, the suspensions were placed on glass slides and treated with polylysine for 1 h. After 1 h, the slides were washed five times with ddH_2O, and the bacteria cells that were attached to the surface were treated with ice-cold trichloroacetic acid (TCA, Sigma-Aldrich) to cause lysis. The internal content of the bacteria was probed with ICP measurements to diagnose whether the NPs had penetrated the bacteria.

Intracellular ROS Assays: For the detection of ROS production upon exposure to Zn:CuO and CuO NPs, the cells were pre-incubated with 10 μM of CM-H_2DCFDA (Invitrogen, Molecular Probes) in PBS for 30 min to allow the dye to enter the cells. This dye freely permeates the cell membrane and becomes fluorescent upon cleavage by ROS. The samples were analyzed for emission at 530 nm using an excitation source at 485 nm. Untreated cells and CM-H_2DCFDA cells pre-incubated with 100 μM H_2O_2 for 30 min were used as the negative and positive controls, respectively.

Lipid Peroxidation Assay: A homogenate was obtained by lysing 5.0×10^6 cells cultured overnight with or without 1 mg/mL of Zn:CuO or CuO NPs with 10% ice-cold TCA. The lysis mixture was centrifuged for 15 s at 14 000 rpm (centrifuge model 5418, Eppendorf).

Aliquots (1 mL) of supernatant were added to 1 mL of 0.6% 2 thiobarbituric acid (TBA, Sigma-Aldrich) and heated in a boiling water bath for 10 min. The samples were cooled, and the chromogenic complex formed by TBA and malondialdehyde-bis-(dimethylacetal)1,1,3,3-tetramethoxypropan (MDA) binding was determined at 535 nm (Ultrospec 2100 pro, Amersham Biosciences).

Acknowledgements

We thank Avi Yosipof from Bar Ilan University, for assistance with the statistical analysis in this study. This research is part of the requirements for a Ph.D. thesis for Michal Eshed at Bar Ilan University. This research was carried out as part of the activities of the KAMIN project financed by the Israeli Ministry of Industry, Trade and Labor to EB.

Received: July 18, 2013
Revised: September 3, 2013
Published online: October 25, 2013

[1] W. J. Loesche, E. Grenier, *J. Dent. Res.* **1976**, *55*, A87.
[2] S. N. Peterson, E. Snesrud, J. Liu, A. C. Ong, M. Kilian, N. J. Schork, W. Bretz, *PLoS One.* **2013**, *8*, 1.
[3] J. A. Aas, B. J. Paster, L. N. Stokes, I. Olsen, F. E. Dewhirst, *J. Clin. Microbiol.* **2005**, *43*, 5721.
[4] E. Zaura, B. J. F. Keijser, S. M. Huse, W. Crielaard, *BMC Microbiol*. **2009**, *9*, 259.
[5] J. Smullen, M. Finney, D. M. Storey, H.A. Foster, *J. Appl. Microbiol.* **2012**, *113*, 964.
[6] S. S. Socransky, A. D. Haffajee, *Periodontology 2000* **2005**, *38*, 135.
[7] W. J. Loesche, *Microbiol Rev.* **1986**, *50*, 353.
[8] V. G. Pol, D. N. Srivastava, O. Palchik, V. Palchik, M. A. Slifkin, A. M. Weiss, A. Gedanken, *Langmuir* **2002**, *18*, 3352.
[9] V. G. Pol, G. Wildermuth, J. Felsche, A. Gedanken, J. Calderon-Moreno, *J. Nanosci. Nanotechnol.* **2005**, *6*, 975.
[10] I. Perelshtein, Y. Ruderman, N. Perkas, J. Beddow, G. Singh, M. Vinatoru, E. Joyce, T. J. Mason, M. Blanes, K. Mollá, A. Gedanken, *Cellulose* **2013**, *20*, 1215.
[11] E. Malka, I. Perelshtein, A. Lipovsky, Y. Shalom, L. Naparstek, N. Perkas, T. Patick, R. Lubart, Y. Nitzan, E. Banin, A. Gedanken, *Small* 2013, DOI: 10.1002/smll.201301081.
[12] M. Eshed, J. Lellouche, S. Matalon, A. Gedanken, E. Banin, *Langmuir* **2012**, *28*, 12288.
[13] M. J. Domek, M. W. LeChevallier, S. C. Cameron, G. A. McFeters, *Appl. Environ. Microbiol.* **1984**, *48*, 289.
[14] S. J. Brookes, R. C. Shore, C. Robinson, S. R. Wood, J. Kirkham, *Arch. Oral. Biol.* **2003**, *48*, 25.
[15] R. V. Oppermann, J. R. Johansen, *Scand. J. Dent. Res.* **1980**, *88*, 476.
[16] J. Afseth, R. V. Oppermann, G. Rolla, *Acta Odontol. Scand.* **1980**, *38*, 229.
[17] R. V. Oppermann, G. Rolla, J. R. Johansen, S. Assev, *Scand. J. Dent. Res.* **1980**, *88*, 389.
[18] J. Afseth, S. M. Amsbaugh, E. Monell- Torrens, W. H. Bowen, G. Rolla, J. Brunelle, E. Dahl, *Caries Res.* **1984**, *18*, 434.
[19] Z. Radovanovic, D. Veljovic, B. Jokic, S. Dimitrijevic, G. Bogdanovic, V. Kojic, R. Petrovic, D. Janackovic, *J. Serb. Chem. Soc.* **2012**, *77*, 1787.
[20] Y. M. Kim, S. Farrah, R. H. Baney, *Electron. J. Biotechnol.* **2006**, *9*, 176.
[21] J. Lellouche, E. Kahana, S. Elias, A. Gedanken, E. Banin, *Biomaterials* **2009**, *30*, 5969.
[22] R. Brayner, R. Ferrari-Iliou, N. Brivois, S. Djediat, M. F. Benedetti, F. Fievet, *Nano Lett.* **2006**, *6*, 866.
[23] S. Makhluf, R. Dror, Y. Nitzan, Y. Abramovich, R. Jelinek, A. Gedanken, *Adv. Funct. Mater.* **2005**, *15*, 1708.
[24] J. T. Seil, T. J. Webster, *Int. J. Nanomed.* **2012**, *7*, 2767.
[25] A. Catala, *Chem. Phys. Lipids* **2009**, *157*, 1.
[26] F. Michel, D. Bonnefont-Rousselot, E. Mas, J. Drai, P. Therond, *Ann. Biol. Clin.* **2008**, *66*, 605.
[27] A. Thill, O. Zeyons, O. Spalla, F. Chauvat, J. Rose, M. Auffan, A. M. Flank, *Environ. Sci. Technol.* **2006**, *40*, 6151.
[28] J. Lovric, S. J. Cho, F. M. Winnik, D. Maysinger, *Chem. Biol.* **2005**, *12*, 1227.
[29] S. Kang, M. Pinault, L. D. Pfefferle, M. Elimelech, *Langmuir* **2007**, *23*, 8670.
[30] G. A. Norton, J. B. Schroeder, G. M. Klody, *Nucl. Instr. Methods Phys. Res. B* **1989**, *40–41*, 785.
[31] N. P. Barradas, C. Jeynes, *Nucl. Instr. Methods Phys. Res. B* **2008**, *266*, 1875.
[32] J. F. Ziegler, *Nucl. Instrum. Methods Phys. Res. B* **2004**, *219*, 1027.
[33] N. P. Barradas, *Nucl. Instrum. Methods Phys. Res. B* **2004**, *225*, 318.
[34] L. Wielopolski, R. P. Gardner, *Nucl. Instrum. Methods Phys. Res.* **1976**, *133*, 303.
[35] A. Gurbich, Institute for Physics and Power Engineering, Obninsk, Russia, Nuclear Data Service, http://www-nds.iaea.org/ibandl/ (2002–2011), accessed: June, 2013.
[36] A. Gurbich, I. Bogdanovic-Radovic, M. Chiari, C. Jeynes, M. Kokkoris, A. R. Ramos, M. Mayer, E. Rauhala, O. Schwerer, S. Liqun, I. Vickridge, *Nucl. Instrum Methods Phys. Res., Sect. B.* **2008**, *266*, 1198.
[37] A. Gurbich, SigmaCalc, calculator provides evaluated (recommended) differential cross sections for Ion Beam Analysis, http://www.surreyibc.ac.uk/sigmacalc/, accessed: June, 2013.
[38] A. F. Gurbich, *Nucl. Instrum. Methods Phys. Res., Sect. B* **2010**, *268*, 1703.
[39] C. Jeynes, N. P. Barradas, P. K. Marriott, G. Boudreault, M. Jenkin, E. Wendler, R. P. Webb, *J. Phys. D: Appl. Phys.* **2003**, *36*, R97.
[40] Ion beam center, http://www.surreyibc.ac.uk/ndf, accessed: June, 2013.
[41] G. Boudreault, C. Jeynes, E. Wendler, A. Nejim, R. P. Webb, U. Watjen, *Surf. Interface Anal.* **2002**, *33*, 478.
[42] N. P. Barradas, K. Arstila, G. Battistig, M. Bianconi, N. Dytlewski, C. Jeynes, E. Kotai, G. Lulli, M. Mayer, E. Rauhala, E. Szilagyi, M. Thompson, *Nucl. Instr. and Meth. in Phys. Res. B* **2008**, *266*, 1338.
[43] C. L. Munro, F. L. Macrina, *Mol. Microbiol.* **1993**, *8*, 133.
[44] S. Croft, *Methods Molec. Biol. Elec. Microsc. Methods Prot.* **1999**, 117.